Light-driven chloride transport kinetics of halorhodopsin

Hasin Feroz[a,1], Bryan Ferlez[b,1], Cecile Lefoulon[c,1], Tingwei Ren[a], Carol S. Baker[b], John P. Gajewski[b], Daniel J. Lugar[b], Sandeep B. Gaudana[d], Peter Butler[e], Jonas Hühn[f], Matthias Lamping[f], Wolfgang J. Parak[f], Julian M. Hibberd[g], Cheryl A. Kerfeld[d,h,i], Nicholas Smirnoff[j], Mike Blatt[c], John H. Golbeck[b,k], Manish Kumar[a,2 ‡]

[a] Department of Chemical Engineering, The Pennsylvania State University, University Park, PA USA
[b] Department of Biochemistry and Molecular Biology, The Pennsylvania State University, University Park, PA USA
[c] Laboratory of Plant Physiology and Biophysics, Institute of Molecular Cell and Systems Biology, Bower Building, University of Glasgow, Glasgow G12 8QQ, UK
[d] MSU-DOE Plant Research Laboratory and Department of Biochemistry and Molecular Biology, Michigan State University, East Lansing, MI, USA
[e] Department of Biomedical Engineering, The Pennsylvania State University, University Park, PA USA
[f] Department of Physics and Chemistry, Philipps University of Marburg, DE
[g] Department of Plant Sciences, University of Cambridge, Cambridge, CB2 3EA, UK
[h] Department of Plant and Microbial Biology, University of California, Berkeley, Berkeley, CA, USA
[i] Molecular Biophysics and Integrated Bioimaging Division, Lawrence Berkeley National Laboratory, Berkeley, CA, USA
[j] School of Biosciences, University of Exeter, Exeter, UK
[k] Department of Chemistry, The Pennsylvania State University, University Park, PA 16802

[1]These authors contributed equally.
[2]Corresponding Author, Department of Chemical Engineering, Pennsylvania State University, 43 Greenberg building, University Park, PA 16802, USA. Phone: +1 814 865 7519. Email: manish.kumar@psu.edu.

Key words

Optogenetics, halorhodopsin, transport rates

ABSTRACT

Despite growing interest in light-driven ion pumps for use in optogenetics, current estimates of their transport rates span two orders of magnitude due to challenges in measuring slow transport processes, determining protein concentration and / or orientation in membranes *in vitro*. In this study, we report the first direct quantitative measurement of light-driven Cl^- transport rates of the anion pump halorhodopsin from *Natronomonas pharaonis* (*Np*HR). We used light-interfaced voltage clamp measurements on *Np*HR-expressing oocytes to obtain a transport rate of 219 (± 98) Cl^-/protein/s for a photon flux of 630 photons/protein/s. The measurement is consistent with the literature reported quantum efficiency of ~30% for *Np*HR, i.e., 0.3 isomerizations per photon absorbed. To reconcile our measurements with an earlier-reported 20 ms rate limiting step or 35 turnover/protein/s, we conducted novel consecutive single-turnover flash experiments that demonstrate that under continuous illumination, *Np*HR bypasses this step in the photocycle as proposed in a recent study by Kleinlogel *et al.*

INTRODUCTION

Optogenetics is an emerging frontier of neuroscience and synthetic biology with applications in therapeutics, drug targeting, and the study of the brain as a complex electronic circuit (1). In some applications, microbial opsins are heterologously expressed in neural cells and used to elicit light-induced hyper/de-polarization of neural membranes in the study of drug addiction (2), depression (3), epilepsy (4), Parkinson's (5), and other neural diseases (1, 5, 6). In addition to their widespread use in optogenetics, opsins are also of interest for use in biophotonic devices such as holographic processors, optical memory, artificial retinas, and photovoltaic devices (7). Despite the growing applications of both natural and genetically-modified light-driven opsins (8, 9), no standard technique exists for direct measurement and comparison of opsin-mediated ion transport rates (10).

The opsin of interest in this study, halorhodopsin from *Natromonas pharaonis* (*Np*HR), is an electrogenic pump that transports Cl^-, Br^-, I^-, NO_3^- and SCN^- vectorially across the lipid membrane in response to light (11). In optogenetics, *Np*HR is specifically used for silencing neurons through its effect on polarizing the neural membrane (12, 13) and to treat rats and potentially humans for retinitis pigmentosa (14). Since its discovery in 1976 (15), studies have focused on the structure of *Np*HR and its mechanism of ion transport (16-20). However little is known about the intrinsic transport rate of this light-driven ion pump, a critical parameter in predicting the extent of opsin-mediated neural polarization (10). One reason for the almost complete lack of data stems from the difficulty in measuring the approximately thousand-fold slower transport rate of light-driven pumps in comparison to well-studied light-gated channels (21, 22).

Currently estimated chloride transport rates for *Np*HR span three orders of magnitude from less than 1 ion/protein/s (18, 23) to as high as 1245 ions/protein/s (24) using various indirect techniques (**Table 1**). The discrepancy in measurements can be explained due to semi-quantitative / indirect methods of measurement of ion transport or protein concentration, challenges in estimating the directionality of proteins in *in vitro* systems and / or differences in illumination conditions. The lowest reported transport rate was determined by using an indirect Cl^- transport measurement in *N. pharaonis* envelope vesicles, which uses passive proton transport in the presence of a proton ionophore to estimate the active transport rate of Cl^- ions (less than 1 ion/protein/s) (18, 23). The next lowest measurement was based on flash optical experiments. From the *Np*HR photocycle model proposed by Chizhov *et al.* (25), the rate-limiting step is proposed to be the final transition between the state P_6 and the ground state, P_0 (**Figure 1**). This is equivalent to a maximum attainable transport rate of ~ 35 Cl^- ions/protein/s ($t_{1/2}$ = 20 ms) (25, 26). However, the kinetic evidence for this final proposed transition is relatively weak compared to the other kinetic intermediates in the photocycle. The absorption spectra of P_6 and P_0 are almost identical and the amplitude of the transient absorption change attributed to this transition only constitutes ~1% of the maximal change in absorbance observed during the photocycle (25).

More recently, Kleinlogel *et al.* used patch clamp current measurements on tandem constructs of *Np*HR and channelrhodopsin (ChR2) in neural cells to estimate a transport rate of 1245 ions/protein/s under continuous illumination (24). To reconcile this faster transport rate, Kleinlogel *et al.* proposed that under continuous illumination, the final step in the photocycle with a half-life of 20 ms ($P_6 \rightarrow P_0$) can be bypassed (**Figure 1)**. On the basis that P_6 and P_0 have nearly identical absorption spectra, they proposed that the last state (P_6) could theoretically absorb a photon of light and initiate another turnover of *Np*HR without passing through the ground state (P_0). We tested this "bypass" hypothesis by exciting detergent-solubilized *Np*HR with repeated flashes of actinic light at increasing repetition rates, to simulate an approach to continuous illumination, while monitoring the recovery of the Cl^- bound state of the excited protein. We monitored the time-dependence of the recovery of *Np*HR by measuring the absorbance change of *Np*HR at 570 nm, which is characteristic of the chloride uptake step, the penultimate step of the photocycle (**Figure 1**). The amplitude of absorbance recovery/change at 570 nm is directly proportional to the fraction of *Np*HR that is able to bind a chloride ion following turnover in response to actinic light. We observed an equivalent amount of absorbance change at 570 nm at actinic repetition rates faster than the slower $P_6 \rightarrow P_0$ transition ($t_{1/2}$ = 20 ms) indicating that the majority of the *Np*HR population is primed and ready to pump the next ion in response to actinic illumination (**Figure 4**). This offers direct evidence for the "bypass" hypothesis and suggests the P_6 to P_0 relaxation is not the rate-limiting step in the *Np*HR photocycle under continuous illumination.

While previous measurements have estimated the Cl^- transport rate of *Np*HR using indirect methods, *a direct quantitative measurement of the Cl^- transport rate of NpHR, to our knowledge, does not exist*. We therefore set out to measure the Cl^- transport rate of directionally inserted *Np*HR with a N-terminal Myc-tag in *Xenopus laevis* oocytes to determine the average per protein transport rate of *Np*HR *in vivo*. We quantified ion transport in oocytes in response to light using voltage clamp measurements and estimated the protein expressed per oocyte by quantifying the genetically fused Myc-tag using Western blot analysis. This analysis provides a transport rate of 219 (± 98) Cl^-/protein/s at a photon flux of 630 photons/protein/s or 0.35 (± 0.16) Cl^-/photon. This per photon transport rate is consistent with the previously reported quantum efficiency of *Np*HR of ~0.3 which corresponds to 0.3 successful isomerizations of *Np*HR per photon absorbed (28-30). We propose that this oocyte-based assay can also be used to directly measure the transport rates of other light-driven opsins. These ion transport rates can be used to guide the optimization of opsin expression to maximize output (e.g. neural (de)polarization) while minimizing photodamage from external illumination (8, 10, 13).

MATERIALS AND METHODS

1. Photocurrent measurement on *Np*HR expressed in oocytes

Construction of the expression plasmid of the histidine-tagged NpHR in the oocyte expression pGT vector. A Gateway BP reaction was used to recombine a N-terminal Myc-tagged and C-terminal 6xHis tag fused *Np*HR into Gateway™ entry vector pDONR207 using BP clonase II (Life Technologies). The resulting entry clone was recombined via an LR reaction (Life Technologies) into pGT-Dest oocyte expression vector described previously by Grefen *et al.* (31). Capped cRNA was synthesized with an *in vitro* transcription kit, T7 mMessage mMachine

(Ambion, USA), from the linearized pGT destination clone.

Expression and ion current measurement of the Myc-tagged NpHR in Xenopus laevis oocytes. The method used was adapted from previous work by Seki e*t al.* and Grefen *et al.* (20, 31). Mature oocytes (stage V-VI) from *Xenopus* were isolated by treatment with collagenase (2 mg/ml), and maintained at 18°C in ND96 medium (2 mM KCl, 96 mM NaCl, 1 mM $MgCl_2$, 1.8 mM $CaCl_2$, 5 mM HEPES, pH 7.4), supplemented with 3 mM retinal and 0.5 µg/ml gentamycin. Oocytes were injected with 3 ng (n=7) and 9 ng (n=10) of *Np*HR cRNA as a control for expression variation with cRNA concentration and incubated for 3 days before recording. Electrophysiological studies were performed with the two-electrode voltage-clamp (TEVC) technique. Oocytes were recorded under continuous perfusion in a solution containing 100 mM NaCl, 2 mM KCl, 1.5 mM $MgCl_2$, 1 mM $CaCl_2$, 10 mM HEPES, pH 7.4. A voltage clamp protocol was run just before and during light stimulation once the membrane potential had stabilized. Illumination at 589 nm was provided by a MGL-F-589nm 100 mW output power (9.9 x 10^{-2} mW/cm^{-2}) laser (CNI Optoelectronics, China). Holding voltage was set at 0 mV, then protocol steps were incrementing from 0 mV to 100 mV, and decreasing from 0 mV to -200 mV. TEVC experiments were performed with Axoclamp 2B amplifier (Axon Instruments) and currents recorded with Henry III software (Y-Science; University of Glasgow). The photoinduced current was calculated as the difference between the steady-state currents recorded before and during light stimulation.

Experimental procedure for determining NpHR concentration in oocytes

Determination of NpHR bound to Myc antibody prior to NpHR quantification in oocyte. Purified Myc- and His- tagged *Np*HR were incubated with c-Myc tag antibody Ab9106 (Abcam) in excess for 9 hours/overnight at 4°C followed by incubation with Ni NTA resin for 2 hours to bind the His-*Np*HR-MycAb complex. Prior to incubation, Ni resin was washed three times with washing buffer (150 mM NaCl, 50 mM Tris, 5% glycerol, 0.2% Triton, pH 8). The resin-*Np*HR-antibody complex was then poured onto a GEN-1SBM-100 mini filter and washed with the same washing buffer for at least 60× the resin volume. The column was then eluted with 150 mM NaCl, Tris 50 mM, 300 mM imidazole solution to obtain pure *Np*HR-antibody complex. The concentration of the purified Myc-tagged *Np*HR was first determined from a Coomassie blue-stained gel using 26 kDa glutathione S-transferase (GST) as a standard to develop a calibration curve (SI **Figure S1A**). *Np*HR-antibody complexes were run on the same gel after denaturation by boiling 9 µL of protein complex with 5 µL DTT-containing loading buffer for 10 min and then incubating the mixture at 37°C for 30 min. Following denaturation, *Np*HR is a 32/100th fraction of the measured 50 kDa antibody subunit. The relative density of this gel was determined using ImageJ v. 1.48 software (http://rsb.info.nih.gov/ij/). Once the recombinant *Np*HR concentration was determined, it was used to determine *Np*HR concentration in oocyte membranes (SI **Figure S1B**).

*Protein quantification in oocytes. Np*HR concentration in oocytes, specifically in the plasma membrane of oocytes, was measured as follows. Oocytes were harvested just after recording; their vittelin membrane removed with forceps and the oocytes incubated for one hour with c-Myc tag antibody (Abcam Ab9106, 0.5 µg/ml). Following incubation with the antibody, the oocytes were washed 3 times in 20 ml ND96 to remove unbound myc-antibody (therefore excluding the possibility of the antibody binding to poorly-trafficked *Np*HR protein not localized on the cell surface). All of the solution was removed and replaced by a RIPA buffer (150 mM

NaCl, 0.25% SDS, 1% NP-40, 1 mM EDTA, 1 mM NaF, 1.125 mM DMFS, 50 mM Tris HCl pH 7.4; 10 µl/oocyte), and then oocytes were homogenized and centrifuged at 425 *g*. One volume of loading buffer (4M urea, 10% SDS, 40 mM EDTA, 0.2% Triton, 0.1% bromophenol blue, 20% glycerol, 200 mM DTT, 100 mM Tris HCl pH 6.8) was added to the supernatant and samples boiled for 10 min before running a gel followed by Western blotting. Membranes were blotted with secondary horseradish peroxidase-coupled goat anti-rabbit antibody (Abcam dilution 1:1000) and bands were detected using ECL Advance Detection Kit (GE Healthcare). The relative density of the developed bands was calculated using Fusion-Capt software (Vilber Lourmat, France) (SI **Figure S1B**).

2. *E. coli* growth and purification of *Np*HR

Expression and purification of *Np*HR was adapted from the protocol of Sato, *et al.* (16). We expressed *Natromonas pharaonis Np*HR by cloning an *Escherichia coli* codon optimized gene with a C- terminal 6x histidine tag (^{1}MAETLP.....TPADD^{291}**LE**HHHHHH]). Using the T7 polymerase/pCDF Duet-1 enhanced co-expression system for *E. coli* BL21 (DE3) (Novagen), we obtained high expression of *Np*HR-LE-his from plasmid pCB8a (16). The cells were grown at 37°C in 2×YT medium supplemented with 50 µg/ml spectinomycin (Gold Biotechnology). At an optical density at 600 nm, OD_{600} of 0.6, 5 µg of all-*trans*-retinal (Sigma-Aldrich) was added per liter of culture and the cells were grown for an additional 4 hours before harvesting. The cell pellet was resuspended in lysis buffer (50 mM Tris-HCl, pH 8.0, 5 mM $MgCl_2$) and lysed in a microfluidizer (M110EH, Microfluidics Corporation). Cell debris was removed via low speed centrifugation (2000 *g*) and the resulting supernatant was spun at 208,000 *g* for 1 h at 4°C to pellet the plasma membranes. The membrane pellets were suspended in 50 mM MES, pH 6.0, 300 mM NaCl, 1.5% DM (n-decyl-β-D maltopyranoside) (GLYCON Biochemicals, Germany) and solubilized overnight at 4°C. Unsolubilized membranes were removed by ultracentrifugation at 208,000 *g* for 1 hour at 4°C. The supernatant was incubated with Ni-NTA resin and the resin washed to remove non-specifically bound proteins with wash buffer (50 mM MES, pH 6.0, 300 mM NaCl, 45 mM imidazole, 0.2% DM). The protein was eluted with a high imidazole elution buffer (50 mM MES, pH 6.0, 300 mM NaCl, 1 M imidazole, 0.2% DM); the final protein concentration and purity was estimated by the molar extinction coefficient (54000 $M^{-1}cm^{-1}$ at 580 nm) and the ratio of 280 nm to 580 nm absorbance (32). We used the Bradford assay for initial quantification of the protein for a standard / calibration curve. A correction factor of 1.684 was applied to the Bradford assay as obtained by determining the purified *Np*HR concentration using the Bradford assay and then quantifying the actual amino acid content of the same protein sample using chemical analysis (details in the website http://msf.ucdavis.edu/amino-acid-analysis/, Molecular Structural Facility, UC Davis) (16, 32, 33). Purity of the isolated protein was confirmed using silver stained SDS-PAGE and anti-histidine tag Western blot analysis which show a single band at ~ 30 kDa (**Figures 2 A and B**). The absorption spectrum of the purified detergent-solubilized *Np*HR has an absorption maximum at 580 nm consistent with all-trans retinal incorporation (**Figure 2 C**) (25, 26).

3. Photocycle measurements of *Np*HR

Consecutive single-turnover flash induced absorbance changes at 570 nm were measured with a JTS-10 pump-probe spectrometer (Bio-logic, Knoxville, TN) with a time resolution of 100 μs per point. The optical sample was contained in a cylindrical cuvette with a 1 cm path length which was loaded with a syringe such that the final sample geometry ruled out the possibility of diffusional replacement of *Np*HR in the optical path on the timescale of our consecutive flash assays. *Np*HR was purified as described above and imidazole was removed from the elution buffer by use of a G-25 size exclusion column (GE healthcare, Little Chalfont, UK) into buffer containing 50 mM MES pH 6.0 with 0.2% n-decyl-β-D-maltopyranoside (Anatrace, Maumee, OH) and 300 mM NaCl at an $OD_{580\ nm}$ of 0.06. Non-saturating excitation at 532 nm was provided by a frequency-doubled ORC-1000 Nd:YAG laser (Clark MXR Inc, Dexter, MI) at 4 mJ/pulse with a pulse width of 400 ns (12.7 MW/cm^{-2}). The probe beam was provided by the internal JTS-10 pulsed white light LED with a pulse width of ~10 μs. The probe beam was filtered prior to passing through the sample using a 570 nm interference filter with a full width at half maximum of 10 nm (Edmund Optics, Barrington, NJ) and the resulting light intensity at 570 nm incident on the sample was ~25 nW/cm^{-2}. The timing of the actinic pulses was controlled externally by a Hewlett Packard 8112A pulse generator (Hewlett Packard, Palo Alto, CA) in external burst mode. The actinic laser was triggered using the JTS-10 100 ms after the start of data collection to obtain a baseline. Data are the result of a single data acquisition with a subtracted dark signal where the laser was fired but the actinic light blocked from exciting the sample to remove a minor electrical background signal generated from the laser (See SI **Figure S2 A,B** for representative raw data). Rare single point deviations from the exponential recoveries due to small air bubbles in the cuvette or misfiring of the detection source in the BioLogic JTS-10 instrument had amplitudes an order of magnitude larger than the rest of the data points and were deleted manually. Only 4 such points were observed out of the 1,784 collected for the entire data set. Consecutive flash experiments using the ORC-1000 Nd:YAG laser (Clark MXR Inc, Dexter, MI) were carried out at 70% of the saturation limit for *Np*HR as limited by the intensity of the actinic source (4 mJ/pulse). A Quanta-ray DCR-11 frequency doubled Nd:YAG laser (Spectra-Physics, Santa Clara, CA) capable of 21 mJ/pulse single-turnover flashes (at 1 Hz repetition rate) was used to measure the saturation percentage of the 570 nm photobleaching signal at 4 mJ/pulse. *Np*HR saturation was obtained at light intensities greater than or equal to 9.7 mJ/pulse as measured by the amplitude of the initial light-induced absorbance change at 570 nm (SI **Figure S3 A, B**).

RESULTS

Voltage-clamp measurements on *Np*HR-expressing oocytes

Voltage-clamp experiments were conducted with *Xenopus laevis* oocytes injected with water or with *Np*HR cRNA to express *Np*HR and subsequently exposed to laser illumination to determine the ion transport rates of *Np*HR (**Figure 3** and **Figure S1**). The per protein ion transport was then determined from measured ion currents at 0 mV and protein concentrations calibrated from Coomassie stained gels and Western blot analyses. Loading concentrations of oocytes expressing *Np*HR were adjusted to operate in the linear range of the Myc-tagged *Np*HR calibration curve and densiometric analysis of the resulting Western blot data used to estimate *Np*HR concentration in the oocyte membrane (34-36). The resulting per protein ion transport was 219 (± 98) Cl^- /protein/s.

Number of photons absorbed per protein. The titration curve of current per oocyte over a range of laser intensities (**Figure S4**) appears to be well below those required for saturation, i.e., for activation of the entire *Np*HR population expressed in oocytes. To obtain ion transport per protein *per photon*, we calculated the number of photons absorbed per protein per second by taking the product of the overall photon flux (I) and the effective chromophore cross-sectional area (σ). The latter is obtained from the molar extinction coefficient (ε) of the chromophore at the excitation wavelength (37). For *Np*HR in the presence of Cl^-, illuminated at 589 nm, $\sigma = 2303 \frac{\varepsilon_{589nm}}{N_A}$ cm^2 $molecule^{-1}$ where the extinction coefficient $\varepsilon_{589nm} = 0.97(\varepsilon_{580nm})$ is derived from the steady-state absorbance spectrum of *Np*HR (32, 37). Thus the data collectively lead to the average transport rate of *Np*HR of 219 (± 98) Cl^-/protein/s for a photon flux of 630 photons/protein/s, i.e., 0.35 (± 0.16) Cl^-/photon.

Consecutive single-turnover flash experiments on *Np*HR *in vitro*

To test the feasibility of our measured steady state Cl^- transport rate in oocytes we set out to determine whether the $P_6 \rightarrow P_0$ step in the *Np*HR photocycle is rate limiting. To do this we interrogated detergent solubilized *Np*HR micelles with a series of consecutive actinic flashes with pulse delay times that were both longer and shorter than the $P_6 \rightarrow P_0$ half-life. As we increase the repetition rate of temporally resolved consecutive flashes we can approach the conditions of continuous illumination used in steady state assays, such as our oocyte experiment, while directly probing whether excitation of *Np*HR in the P_6 state can lead to another turnover. For example, at excitation repetition rates greater than 50 Hz (< 20 ms between each consecutive flash), *Np*HR is excited faster than the decay of $P_6 \rightarrow P_0$, which has a half-life of 20 ms (**Figure 1)**. If the $P_6 \rightarrow P_0$ step is rate-limiting, consecutive actinic flashes at > 50 Hz should elicit only fractional amounts of absorbance change at 570 nm (due only to the small ~30% of *Np*HR molecules not excited on the first flash, see Materials and Methods and SI **Figure S3**) compared to that following the first actinic pulse as the cycle would not be complete by the time of the next actinic flash. As a consequence, the amplitude of the 570 nm absorbance change will be proportional to the fraction of *Np*HR population that has completed this final step of the photocycle. If the penultimate step in the photocycle of *Np*HR (the chloride uptake step or $P_5 \rightarrow P_6$) for which the half-life of 1.5 ms (**Figure 1**) is rate-limiting, consecutive actinic flashes provided at any rate between 20 and 200 Hz (5-50 ms between each consecutive flash) should all elicit an equivalent light-induced absorbance change at 570 nm because this step remains faster than the excitation rate. **Figure 4** depicts the results of single-turnover flash experiments using detergent-solubilized *Np*HR micelles at 570 nm with varying actinic repetition rates: 20 Hz (dash-dotted line, 50 ms between flashes), 50 Hz (dashed line, 20 ms between flashes), 100 Hz (dotted line, 10 ms between flashes) and 200 Hz (solid line, 5 ms between flashes). In these experiments, each actinic flash generated an absorbance change equal to 93-97% of the amplitude of the first flash in each respective sequence regardless of repetition rate, suggesting that the penultimate Cl^- uptake step ($P_5 \rightarrow P_6$) and not the final protein relaxation step ($P_6 \rightarrow P_0$) is rate-limiting under conditions approaching continuous illumination. Moreover, if the excitation repetition rate is increased to 500 Hz (2 ms between each consecutive flash), an interval more frequent than the chloride uptake step, each

excitation beyond the first exhibits a reduced absorbance change that on average is equal to 81% of that measured for the first flash (SI **Figure S5**).

DISCUSSION

The photocycle of halorhodopsin from *N. pharaonis* has been characterized as consisting of six kinetically distinguishable steps (**Figure 1**), with each intermediate state of the *Np*HR protein labeled as P_0-P_6, where P_0 represents the ground state of *Np*HR before excitation by light (25). The photocycle is initiated by a photon of light promoting the transition from P_0 to the state P_1 (25). The half-lives of the different steps of the photocycle reported by Chizov *et al.* are depicted in **Figure 1**. These half-lives were determined from global fitting with six exponents; the maximum number of exponents needed to obtain the least standard deviation of the weighted residual (25).

From single-turnover flash optical measurements reported in literature, the sixth and final kinetic step ($t_{1/2}$ = 20 ms, $P_6 \rightarrow P_0$) responsible for the regeneration of the ground state (P_0) is predicted to be rate-limiting, suggesting a maximum turnover rate of ~ 35 Cl^- ions/protein/s (25). On the other hand, optogenetic experiments utilizing *Np*HR to hyper / depolarize neural cells under continuous illumination have suggested transport rates of up to 1245 Cl^- ions/protein/s (24). Kleinlogel *et al.* suggested that this discrepancy could be explained if under continuous illumination excitation of P_6, whose absorption spectra is almost identical to the ground state (P_0), could directly lead to generation of P_1 by absorption of a photon, thereby bypassing the ground state (**Figure 1**).

We tested the hypothesis that continuous illumination allows a bypass of the P_0 state by monitoring the P_5 to P_6 transition corresponding to the chloride uptake step of detergent solubilized *Np*HR. These experiments were performed with actinic flashes at varying repetition rates approaching continuous illumination while monitoring the absorbance change at a wavelength characteristic of the uptake of chloride into the active site (570 nm) (**Figure 4**). The half-life of the $P_6 \rightarrow P_0$ transition is 20 ms (50 Hz) and therefore at excitation rates greater than 50 Hz, e.g., 200 Hz (5 ms between each consecutive excitation), the majority of the *Np*HR molecules excited on the first laser flash are still in the P_6 state at the time of the second flash (at t = 5 ms). The second laser flash therefore probes primarily *Np*HR in the P_6 state. If the $P_6 \rightarrow P_0$ step were rate-limiting, then a second actinic flash fired less than 20 ms after the first would yield no significant absorbance change at 570 nm. However, we observe a similar change in absorbance following each actinic flash regardless of the excitation repetition rate; this is consistent with the hypothesis that excitation of P_6 with light can lead to direct generation of P_1. Alternatively, if the slow ~20 ms transition assigned to the decay of the P_6 state by Chizov *et al.* represents a minor off-pathway reaction and not an obligatory intermediate between the chloride uptake step (P_5) and the ground state (P_0), excitation of *Np*HR at pulse intervals between 5-20 ms would similarly lead to equivalent amounts of photobleaching following each flash. Although our data cannot distinguish between these two possibilities, they unambiguously show that the rate-limiting step of the *Np*HR photocycle is not the previously proposed P_6 to P_0 state with a half-life of 20 ms. Therefore in either case we would expect the next longest step (i.e. the chloride uptake step, $t_{1/2}$ = 1.5 ms) to be rate-limiting.

If the photocycle kinetics are an indication of *Np*HR turnover rate, then under continuous illumination, the P_5 to P_6 (or P_0) transition with a half-life of ~ 1.5 ms (~ 460 turnovers/protein/s) is within two fold of our reported transport rate of 219 (± 98) ions/protein/s (**Figure 5A**). Our oocyte-based measurement of 219 (± 98) Cl^-/protein/s at 630 photons/protein/s and that reported for *Np*HR-ChR2 tandem constructs of 1245 Cl^- ions/protein/s at a calculated photon flux of ~3600 photons/protein/s (24) are also within an order of magnitude of each other; the difference between them could be attributed to differences in the photon fluxes employed or methods of protein quantification. Normalizing the rates with respect to photon flux results in per photon ion transport rates of 0.35 (± 0.16) Cl^-/photon (this work) and 0.33 Cl^-/photon (24) showing overlap in the two measurements (24) (**Figure 5B**). The photon flux normalized per protein transport rate is also in agreement with literature-reported quantum efficiencies of *Np*HR which include 0.27 (30), 0.3 (28) and 0.34 (29) based on transient absorbance spectroscopy of *Np*HR (28-30). The *Np*HR transport rates and corresponding quantum yields (ions per photon) from different techniques are summarized in **Figure 5**.

To conclude, we have reported the first direct measurement of the ion transport rate of *Np*HR in *Np*HR-expressing oocytes and confirmed our measurements with consecutive flash photocycle optical experiments. Our *in vivo* ion transport rate measured in *Np*HR-expressing oocytes resulted in 219 (± 98) Cl^-/protein/s for a photon flux of 630 photons/protein/s. Considering the per photon count, our measurement yields a transport rate of 0.35 (± 0.16) Cl^-/photon which is in agreement with the literature-reported quantum yield of *Np*HR of 0.3 and per photon transport rate of 0.33 Cl^-/photon for ChR2-*Np*HR tandem constructs by Kleinlogel *et al.* Further, to reconcile our measurement with inferred *Np*HR turnover of 35/s from the previously-reported slowest step in the photocycle, we carried out consecutive single-turnover flash experiments *in vitro* at different repetition rates. Our data suggests that the previously reported P_6 to P_0 transition is not the rate limiting step in the *Np*HR photocycle and are consistent with the "bypass" hypothesis proposed by Kleinlogel *et al.*, which suggested that under continuous illumination the *Np*HR photocycle short-circuits the P_6 to P_0 transition(24). Alternatively, our data are also consistent with a photocycle model where the P_5 state decays directly to P_0 with a half-life of ~1.5 ms. In the latter model the previously reported P_6 state may still exist but as an off-pathway reaction rather than a required intermediate in the regeneration of P_0. If we assume that the rest of the photocycle remains unaltered, both models predict that the turnover from the chloride uptake step with a half-life of 1.5 ms is ~ 460 turnovers/protein/s. Our measured transport rate of 219 (± 98) Cl^-/protein/s from voltage clamp experiments is within two fold of this turnover. We propose this *in vivo* method to measure ion transport under different illumination intensities can be used to screen optogenetically relevant opsins and predict their efficacy at polarizing neuronal membranes thus providing a standard measurement for single protein biophysical characterization. Recent efforts to engineer *Np*HR to red-shift the absorption spectrum of *Np*HR to improve photon-capture at longer wavelengths (8) or to synthesize photovoltaic devices using bacteriorhodopsin (7) are other novel applications where this assay could prove critical to screen and optimize opsin activity.

Author contributions.

HF designed research; performed research; analyzed photocurrent data and related it to the flash photolysis data; compiled and wrote the paper; BF designed research; performed research; analyzed and wrote the flash experimental portion of paper; CL designed research; performed research, analyzed and contributed to writing the photocurrent portion of the paper; TR

performed research (protein purification and processing); CSB performed research (cloning), contributed to writing sections of paper; JPG performed research to purify protein; DJL performed research to purify protein; SBG contributed to analysis of data; PB contributed analytic tools, JH performed research, ML performed research; WJP designed research, contributed analytic tools; JMH contributed to design of research; CAK contributed to design of research; NS contributed to design of research; MB contributed to design of research, contributed analytic tools for photcurrent measurements, contributed to writing the paper; JHG contributed analytic tools for flash photolysis experiments, contributed to writing the paper; MK designed research, analyzed data, contributed analytic tools for the experiments, wrote and compiled the paper.

Acknowledgements. We thank Shared Fermentation Facility (The Huck Institutes of The Life Sciences, Pennsylvania State University) for support with the protein purification and National Science Foundation for providing funding (PIs: John Golbeck and Manish Kumar) through grant MCB-1359634 and (PIs: Cheryl Kerfeld) through grant MCB-1359636. Parts of the project were supported by the German Research Foundation (DFG grant 794/21-1 to WJP). Michael Blatt acknowledges support from grants BB/M01133X/1, BB/M001601/1 and BB/L019025/1 from the UK Biotechnology and Biological Sciences Research Council. We thank Cory Jones for critical reading of the manuscript and editorial comments and Karim Walters for technical support.

REFERENCES

1. Deisseroth K (2011) Optogenetics. *Nature Methods* 8(1):26-29.
2. Lobo MK*, et al.* (2010) Cell type–specific loss of BDNF signaling mimics optogenetic control of cocaine reward. *Science* 330(6002):385-390.
3. Covington HE*, et al.* (2010) Antidepressant effect of optogenetic stimulation of the medial prefrontal cortex. *The Journal of neuroscience* 30(48):16082-16090.
4. Tønnesen J, Sørensen AT, Deisseroth K, Lundberg C, & Kokaia M (2009) Optogenetic control of epileptiform activity. *Proceedings of the National Academy of Sciences* 106(29):12162-12167.
5. Kravitz AV*, et al.* (2010) Regulation of parkinsonian motor behaviours by optogenetic control of basal ganglia circuitry. *Nature* 466(7306):622-626.
6. Tye KM & Deisseroth K (2012) Optogenetic investigation of neural circuits underlying brain disease in animal models. *Nature Reviews Neuroscience* 13(4):251-266.
7. Wagner NL, Greco JA, Ranaghan MJ, & Birge RR (2013) Directed evolution of bacteriorhodopsin for applications in bioelectronics. *Journal of The Royal Society Interface* 10(84):20130197.
8. Zhang F*, et al.* (2008) Red-shifted optogenetic excitation: a tool for fast neural control derived from Volvox carteri. *Nature neuroscience* 11(6):631-633.
9. Chuong AS*, et al.* (2014) Noninvasive optical inhibition with a red-shifted microbial rhodopsin. *Nature neuroscience* 17(8):1123.
10. Mattis J*, et al.* (2012) Principles for applying optogenetic tools derived from direct comparative analysis of microbial opsins. *Nature Methods* 9(2):159-172.
11. Yizhar O, Fenno L, Zhang F, Hegemann P, & Diesseroth K (2011) Microbial opsins: a family of single-component tools for optical control of neural activity. *Cold Spring Harbor Protocols* 2011(3):top102.
12. Zhang F*, et al.* (2007) Multimodal fast optical interrogation of neural circuitry. *Nature* 446(7136):633-639.
13. Han X & Boyden ES (2007) Multiple-color optical activation, silencing, and desynchronization of neural activity, with single-spike temporal resolution. *PloS one* 2(3):e299.
14. Bourzac K (February 19, 2016) In First Human Test of Optogenetics, Doctors Aim to Restore Sight to the Blind. in *Biomedicine MIT Technology Review*.
15. Matsuno-Yagi A & Mukohata Y (1977) Two possible roles of bacteriorhodopsin; a comparative study of strains of *Halobacterium halobium* differing in pigmentation. *Biochemical and biophysical research communications* 78(1):237-243.
16. Sato M, Kanamori T, Kamo N, Demura M, & Nitta K (2002) Stopped-flow analysis on anion binding to blue-form halorhodopsin from Natronobacterium pharaonis: comparison with the anion-uptake process during the photocycle. *Biochemistry* 41(7):2452-2458.
17. Bálint Z, Lakatos M, Ganea C, Lanyi JK, & Váró G (2004) The nitrate transporting photochemical reaction cycle of the pharaonis halorhodopsin. *Biophysical Journal* 86(3):1655-1663.
18. Schobert B & Lanyi JK (1982) Halorhodopsin is a light-driven chloride pump. *Journal of Biological Chemistry* 257(17):10306-10313.

19. Hazemoto N, Kamo N, Kobatake Y, Tsuda M, & Terayama Y (1984) Effect of salt on photocycle and ion-pumping of halorhodopsin and third rhodopsinlike pigment of Halobacterium halobium. *Biophysical Journal* 45(6):1073-1077.
20. Seki A*, et al.* (2007) Heterologous Expression of *Pharaonis* Halorhodopsin in *Xenopus laevis* Oocytes and Electrophysiological Characterization of Its Light-Driven Cl^- Pump Activity. *Biophysical journal* 92(7):2559-2569.
21. Nagel G*, et al.* (2003) Channelrhodopsin-2, a directly light-gated cation-selective membrane channel. *Proceedings of the National Academy of Sciences* 100(24):13940-13945.
22. Gadsby DC (2009) Ion channels versus ion pumps: the principal difference, in principle. *Nature Reviews Molecular Cell Biology* 10(5):344-352.
23. Duschl A, Lanyi JK, & Zimanyi L (1990) Properties and photochemistry of a halorhodopsin from the haloalkalophile, Natronobacterium pharaonis. *Journal of Biological Chemistry* 265(3):1261-1267.
24. Kleinlogel S*, et al.* (2011) A gene-fusion strategy for stoichiometric and co-localized expression of light-gated membrane proteins. *Nature methods* 8(12):1083-1088.
25. Chizhov I & Engelhard M (2001) Temperature and halide dependence of the photocycle of halorhodopsin from Natronobacterium pharaonis. *Biophysical Journal* 81(3):1600-1612.
26. Hohenfeld IP, Wegener AA, & Engelhard M (1999) Purification of histidine tagged bacteriorhodopsin, *pharaonis* halorhodopsin and *pharaonis* sensory rhodopsin II functionally expressed in *Escherichia coli*. *FEBS letters* 442(2):198-202.
27. Feldbauer K*, et al.* (2009) Channelrhodopsin-2 is a leaky proton pump. *Proceedings of the National Academy of Sciences* 106(30):12317-12322.
28. Arlt T, Schmidt S, Zinth W, Haupts U, & Oesterhelt D (1995) The initial reaction dynamics of the light-driven chloride pump halorhodopsin. *Chemical physics letters* 241(5):559-565.
29. Oesterhelt D, Hegemann P, & Tittor J (1985) The photocycle of the chloride pump halorhodopsin. II: Quantum yields and a kinetic model. *The EMBO journal* 4(9):2351.
30. Kandori H, Yoshihara K, Tomioka H, & Sasabe H (1992) Primary photochemical events in halorhodopsin studied by subpicosecond time-resolved spectroscopy. *The Journal of Physical Chemistry* 96(14):6066-6071.
31. Grefen C*, et al.* (2010) A novel motif essential for SNARE interaction with the K+ channel KC1 and channel gating in Arabidopsis. *The Plant Cell* 22(9):3076-3092.
32. Scharf B & Engelhard M (1994) Blue halorhodopsin from Natronobacterium pharaonis: wavelength regulation by anions. *Biochemistry* 33(21):6387-6393.
33. Facility AAAMS (2017) http://msf.ucdavis.edu/amino-acid-analysis/.
34. Murphy RM & Lamb GD (2013) Important considerations for protein analyses using antibody based techniques: down-sizing Western blotting up-sizes outcomes. *The Journal of physiology* 591(23):5823-5831.
35. Taylor SC & Posch A (2014) The design of a quantitative western blot experiment. *BioMed research international* 2014.
36. Janes KA (2015) An analysis of critical factors for quantitative immunoblotting. *Science signaling* 8(371):rs2.
37. Blankenship RE (2014) *Molecular mechanisms of photosynthesis* (John Wiley & Sons).

TABLES

Table 1. Summary of *Np*HR transport rates from literature

Technique	Estimated transport rates (Cl^- ions/ protein/s)	Methodology
pH measurements in *N. pharaonis* envelope vesicles[23]	<1	Indirect measurement based on secondary transport of protons across the bilayer, estimation of protein concentration using the Lowry method[18].
Single-turnover flash optical experiments[25]	35	Theoretical estimate of the *Np*HR transport rate under single flash conditions assuming the transition of P_6 to ground state (P_0) is rate-limiting. Actual rate may be limited by effective photon flux or ion transport quantum efficiency[10].
Patch-clamp measurement on neural cells expressing tandem construct of ChR2-EYFP-*Np*HR[24]	1245	Overall transport rate for *Np*HR determined from patch clamp ion measurements under continuous orange light. Number of *Np*HR proteins per cell determined using transport measurements of Channel rhodopsin (ChR2) expressed in tandem with *Np*HR divided by earlier reported single channel ChR2 currents extrapolated to experimental conditions (27).

FIGURE LEGENDS

Figure 1. Kinetic Model of the *Np*HR photocycle. Photocycle model adapted from Chizhov *et al.* (25), where P_0 represents the ground state of *Np*HR and P_1-P_6 are six kinetically distinguishable intermediates. Corresponding half-lives for each transition listed between corresponding intermediates. A photon of light initiates the photocycle by promoting the transition between P_0 and P_1. The last and the longest step in this process, the transition from P_6 to the ground state (P_0) with a half-life of 20 ms, is currently accepted to be the rate-limiting step. The "bypass" hypothesis suggests that P_6 can absorb a photon of light and directly transition to P_1, bypassing P_0, under continuous illumination.

Figure 2. Purification and characterization of *Np*HR. A. Silver stained SDS-PAGE and **B.** Anti-histidine tag Western blot show a single band around 30 kDa consistent with the *Np*HR monomeric molecular weight. **C.** Absorbance spectrum of purified *Np*HR with an absorbance maximum at 580 nm.

Figure 3. Determination of the per protein transport rate of *Np*HR expressed in oocytes from *Np*HR-induced photocurrents in a voltage clamp set-up and *Np*HR quantification using Coomassie and Western blot analysis. A. Determination of concentration of detergent-solubilized Myc-tagged *Np*HR from Coomassie gel analysis of *Np*HR-anti-Myc-antibody complex. The gel can be found in SI **Figure S1A**. Densitometry analysis was conducted on the gel band corresponding to the 50 kDa heavy chain of the antibody following denaturation of the *Np*HR-antibody complex and compared against a Coomassie calibration curve obtained with different known concentrations of 26 kDa glutathione S-transferase (GST). **B.** Determination of Myc-tagged *Np*HR expression in oocyte membranes using Western blot analysis. The gel can be found in SI **Figure S1B**. A calibration curve of a range of known concentrations of denatured *Np*HR-antibody complex was used to determine the concentration of *Np*HR per oocyte. The

curve was obtained from a calibration curve of the band intensity from a Western blot analysis on independently purified Myc-tagged *Np*HR proteins. The band intensity was observed to reach saturation at the higher concentrations of purified *Np*HR, and only concentrations for which the calibration curve was linear were used to obtain the concentration of *Np*HR expressed in oocytes. Two different cRNA concentrations were used per batch of oocytes to induce different levels of *Np*HR expression. Each cRNA concentration was treated as a replicate. Two different batches of oocytes were thus tested resulting in 4 replicates. **C.** The current induced in *Np*HR-expressing oocytes was determined using two electrode voltage clamp on oocytes during illumination by a 589 nm laser. Normalizing the current at zero potential from **C.** with corresponding *Np*HR per oocyte from **B.** results in an average transport rate of 0.35 (± 0.16) ions/protein/photon/s. Current recordings were obtained from 7 to 9 oocytes per cRNA injection per oocyte batch.

Figure 4. High-repetition consecutive singe-turnover flash experiments on detergent-solubilized *Np*HR micelles. Detergent-solubilized *Np*HR micelles purified from *E. coli* were illuminated with consecutive actinic flashes at repetition rates of 20 Hz (50 ms between flashes, dash-dotted line), 50 Hz (20 ms between flashes, dashed line), 100 Hz (10 ms between flashes, dotted line), and 200 Hz (5 ms between flashes, solid line). The resulting light-induced changes in absorbance at 570 nm, representative of the chloride uptake step, were recorded as a function of time. Each trace is the difference between a single data collection with and without actinic pulses at the specified repetition rate. Arrows indicate actinic flash events at an intensity of 4 mJ/pulse at 532 nm. The amplitudes of the consecutive absorbance change events at 570 nm are comparable at all excitation rates tested including the 100 Hz and the 200 Hz repetition rates, which are more frequent than the P_6 to P_0 half-life duration ($t_{1/2}$ = 20 ms).

Figure 5. *Np*HR transport rates obtained from voltage clamped current measurements on *Np*HR expressing oocytes (this study) compared with indirectly measured or inferred transport rates and quantum yields from different techniques reported in literature. The normalized per photon oocyte-based transport rate of *Np*HR of 0.35 (± 0.16) Cl^-/photon obtained for an *Np*HR transport rate of 219 (± 98) Cl^-/protein/s for a photon flux of 630 photons/protein/s, is in agreement with the reported quantum yield of *Np*HR of 0.3. The measured value is also in agreement with the electrophysiology-based per photon estimates on tandem fusion constructs of *Np*HR with ChR2 which resulted in a transport rate of 0.33 Cl^-/photon or 1245 ions/protein/s at a photon flux of 3600 photons/protein/s (24).

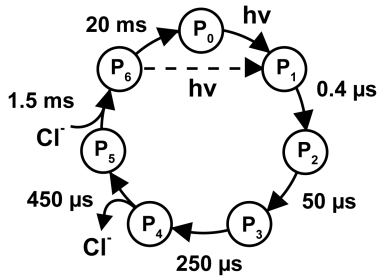

FIGURE 1

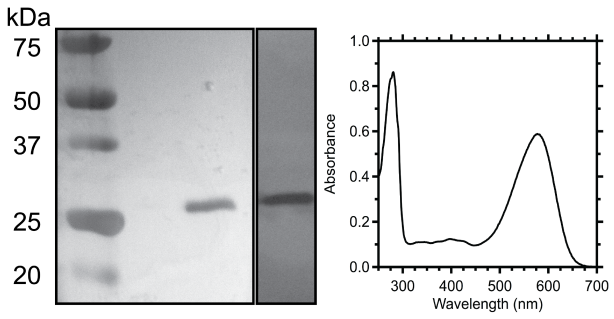
kDa
75
50
37
25
20
Absorbance
1.0
0.8
0.6
0.4
0.2
0.0
300
400
500
600
700
Wavelength (nm)

FIGURE 2

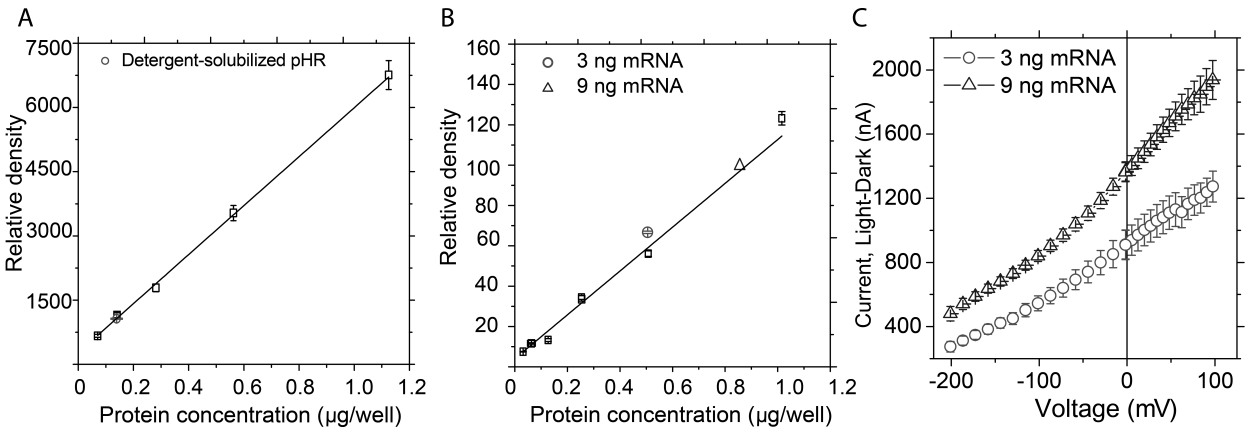
A
Detergent-solubilized pHR
Relative density
Protein concentration (µg/well)
B
3 ng mRNA
9 ng mRNA
Relative density
Protein concentration (µg/well)
C
3 ng mRNA
9 ng mRNA
Current, Light-Dark (nA)
Voltage (mV)

FIGURE 3

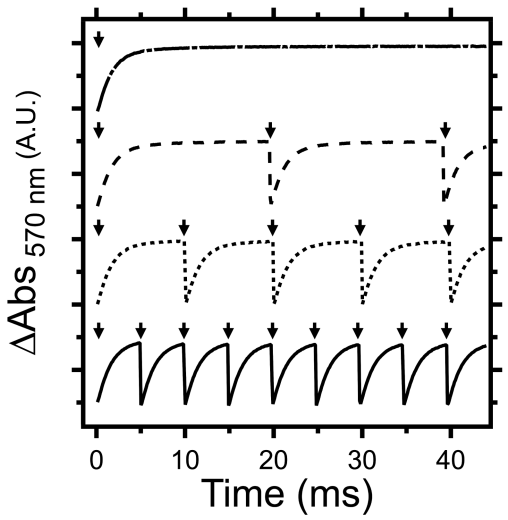

FIGURE 4

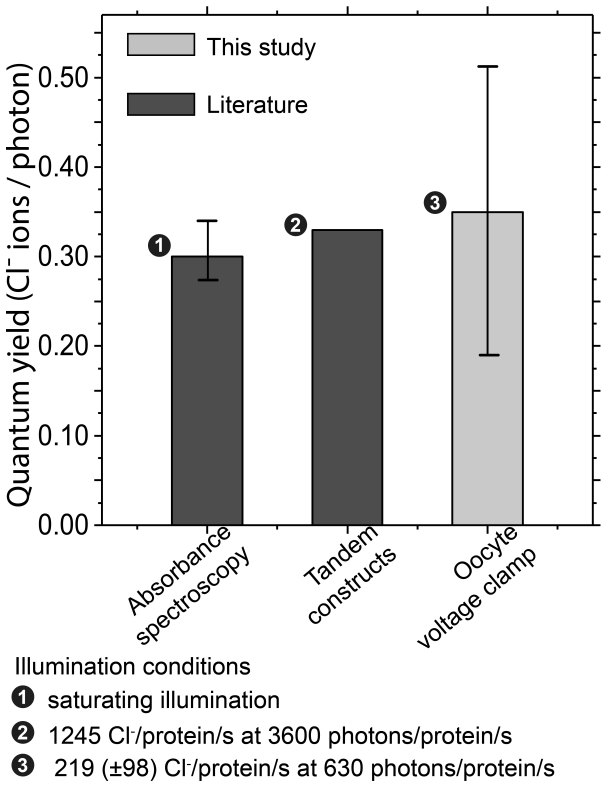
This study
Literature
Quantum yield (Cl- ions / photon)
0.00
0.10
0.20
0.30
0.40
0.50
1
2
3
Absorbance spectroscopy
Tandem constructs
Oocyte voltage clamp
Illumination conditions
1 saturating illumination
2 1245 Cl-/protein/s at 3600 photons/protein/s
3 219 (±98) Cl-/protein/s at 630 photons/protein/s

FIGURE 5